Applied Physics Letters

Synthetic antiferromagnetic layer based on Pt/Ru/Pt spacer layer with 1.05 nm interlayer exchange oscillation period for spin–orbit torque devices

Cite as: Appl. Phys. Lett. **119**, 142401 (2021); https://doi.org/10.1063/5.0063317
Submitted: 13 July 2021 . Accepted: 21 September 2021 . Published Online: 04 October 2021

Yoshiaki Saito, Shoji Ikeda and Tetsuo Endoh

Applied Physics Letters ARTICLE scitation.org/journal/apl

Synthetic antiferromagnetic layer based on Pt/Ru/Pt spacer layer with 1.05 nm interlayer exchange oscillation period for spin–orbit torque devices

Cite as: Appl. Phys. Lett. **119**, 142401 (2021); doi: 10.1063/5.0063317
Submitted: 13 July 2021 · Accepted: 21 September 2021 ·
Published Online: 4 October 2021

Yoshiaki Saito,[1,a] Shoji Ikeda,[1,2,3,4] and Tetsuo Endoh[1,2,3,4,5]

AFFILIATIONS

[1]Center for Innovative Integrated Electronic Systems, Tohoku University, Sendai 980-0845, Japan
[2]Center for Spintronics Research Network, Tohoku University, Sendai 980-8577, Japan
[3]Center for Science and Innovation in Spintronics, Tohoku University, Sendai 980-8577, Japan
[4]Research Institute of Electrical Communication, Tohoku University, Sendai 980-8577, Japan
[5]Department of Electrical Engineering, Graduate School of Engineering, Tohoku University, Sendai 980-8579, Japan

[a)]Author to whom correspondence should be addressed: ysaito@cies.tohoku.ac.jp

ABSTRACT

We investigated interlayer exchange coupling through Pt/Ru/Pt and Pt/Ru multilayers as candidates of nonmagnetic spacer layers in the synthetic antiferromagnetic (AF) layer, which is available for studying AF spintronics using current-induced spin–orbit torque (SOT) switching originating from the spin Hall effect. The AF interlayer exchange coupling with the oscillation period of $\Lambda_2 \sim 1.05$ nm was observed even for the face-centered cubic (fcc) Pt (t_{Pt})/hexagonal Ru/fcc Pt (t_{Pt}) nonmagnetic spacer layer structures in the wide range of both Pt and total nonmagnetic spacer layer thicknesses ($0 \leq t_{Pt} \leq 0.8$ nm, $1.0 \leq t_{total} \leq 2.3$ nm), which would be useful for the systematic investigation of the SOT on the AF structure. Moreover, we observed the disappearance of the one oscillation period ($\Lambda_1 \sim 1.65$ nm) in the case of Pt(111)/Ru(0001) and Pt(111)/Ru(0001)/Pt(111) spacer layers, whereas the existence of two oscillation periods of AF interlayer exchange coupling ($\Lambda_1 \sim 1.65$ nm and $\Lambda_2 \sim 1.05$ nm) in the case of Ru spacer layer was observed. We expect that the Pt/Ru/Pt spacer layer with the oscillation period of $\Lambda_2 \sim 1.05$ nm will pave a way to the AF spintronics based on the multilayer systems.

Antiferromagnetic (AF) materials[1–16] have attracted attention due to their fast magnetization dynamics using current-induced spin–orbit torque (SOT) originating from the spin Hall effect (SHE),[17–36] low magnetic susceptibility, and lack of magnetic stray field. Up to now, several works reported the manipulation of AF structures using electric current.[3,7–16] The manipulation of AF structures in the bulk AF materials, such as CuMnAs, was demonstrated using current-induced internal fields originating from its crystal structure with broken inversion symmetry.[7] Nickel oxide (NiO) is another bulk AF material, and its antiferromagnetically coupled magnetic moments (Néel vector) could be switched by using SOT originating from SHE by utilizing the two Pt layers adjacent to the outside of the NiO layer.[8] Thus, most studies of AF spintronics have focused on bulk AF materials.

On the other hand, a metallic superlattice having an AF structure, in which the ferromagnetic layers separated by the nonmagnetic spacer layer are antiferromagnetically coupled through interlayer exchange coupling (synthetic AF coupling layers),[37,38] was proposed as another candidate system for studying AF spintronics using current-induced SOT switching originating from the SHE.[16,39,40] Ru is the most popular spacer layer for the synthetic AF coupling and has been usually used for many applications. However, because Ru has small SHE (spin Hall angle: $\theta_{SH} \sim 0.6\%$),[41] the use of two Pt layers adjacent to the outside of the synthetic AF coupling layer and utilization of the relatively large SHE of the two adjacent Pt layers ($\theta_{SH} \sim 6\%$–10%)[40,42–45] in Pt/Co/Ru/Co/Pt multilayers[39] have been proposed. However, in the case of the idea of Ref. 39, considering an application of SOT-magnetic random-access memory (MRAM) shown in Fig. 1(a), the Pt layer insertion between the synthetic AF coupling layer and a read device, such as magnetic tunnel junction (MTJ), is not preferable to control the magnetization direction of the

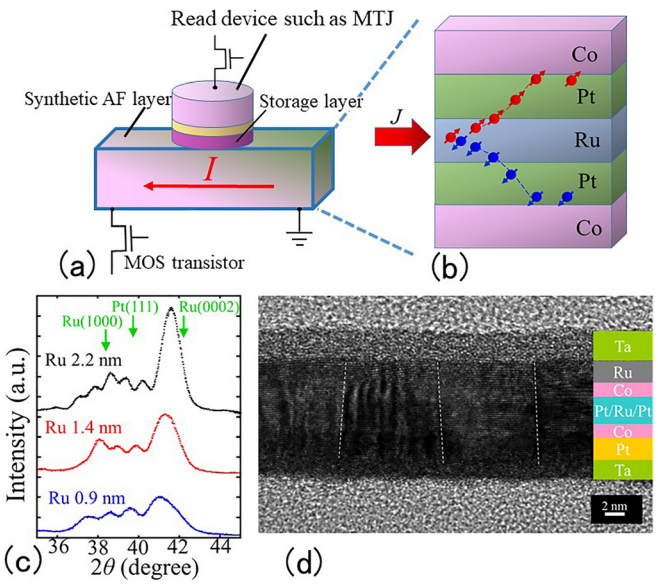

FIG. 1. (a) Schematic diagram for memory cell of spin–orbit torque (SOT)-MRAM with metal-oxide-semiconductor (MOS) transistors and the synthetic antiferromagnetic (AF) layer. The red arrow shows the current (I) direction. (b) The proposed synthetic AF coupling layer structure with the Pt/Ru/Pt nonmagnetic spacer layer. (c) Typical t_{Ru} dependence of out-of-plane XRD results for sample D ($t_{Ru} = 0.9$, 1.4, and 2.2 nm). (d) Cross-sectional transmission electron microscopy image for sample A ($n = 1$, $t_{Co} = 1.1$ nm, $t_{Pt} = 0.8$ nm, and $t_{Ru} = 0.7$ nm). The white dotted lines in (d) are the positions of the grain boundary.

storage layer in the read device by utilizing the exchange interaction between the storage and the synthetic AF coupling layer. Masuda *et al.* proposed the material of Ir-doped Cu alloy (Cu-Ir)[16] for the nonmagnetic spacer layer in the synthetic AF coupling layer of Co/Cu-Ir/Co and observed the AF coupling through $Cu_{95}Ir_5$ alloy with a relatively large SHE ($\theta_{SH} = 3\%$–4%) in the thickness (t_{CuIr}) range of $0.6 < t_{CuIr} < 1.0$ nm. These findings of Ref. 16 have advantages in terms of the magnetization direction control of the storage layer; however, from the viewpoint of passing most of the current through the spacer layer in the synthetic AF coupling layer for SOT switching, the maximum thickness of t_{CuIr}, which shows AF coupling, is relatively thin (maximum thickness is $t_{CuIr} = 1.0$ nm). If one can find an exhibiting AF interlayer exchange coupling through a relatively thicker spacer layer in Co/Pt/Ru/Pt/Co system, this Pt/Ru/Pt spacer layer would be one of promising material for the systematic investigation of the SOT on the AF structure, because one can use the large SHE in Pt layers ($\theta_{SH} \sim 6\%$–10%)[40,42–45] and the exchange interaction between the storage layer and the synthetic AF coupling layer for controlling the magnetization direction of the storage layer in the read device shown in Fig. 1(a).

In this study, we try to investigate Pt/Ru/Pt and Pt/Ru nonmagnetic spacer layers sandwiched by Co layers. The crystal structures of Ru and Pt are hexagonal and face-centered-cubic (fcc), respectively; therefore, it was not clear if there is interlayer exchange coupling through the Pt/Ru/Pt spacer layer. We investigated detailed interlayer exchange coupling through Pt/Ru/Pt and Pt/Ru multilayers as candidates of nonmagnetic spacer layers in the synthetic AF layer and found the AF interlayer exchange coupling through Pt/Ru/Pt and Pt/Ru multilayers.

We prepared many samples with various film stacks by rf magnetron sputtering on oxidized Si substrates. Base pressure of the sputtering system is less than 1×10^{-6} Pa. Details of sample structure (stack) are shown in Table I. In order to confirm the magnetic and interlayer exchange coupling properties, we prepared Ta/Pt(3)/[Co(t_{Co})/Pt(t_{Pt})/Ru(t_{Ru})/Pt(t_{Pt})]$_n$/Co(t_{Co})/Ru(1)/Ta(2) (sample A) (n: repetition number) [Fig. 1(b) shows the case of $n = 1$], Ta/Pt(3)/[Co(t_{Co})/Ru(t_{Ru})/Pt(t_{Pt})]$_n$/Co(t_{Co})/Ru(1)/Ta(2) (sample B) with various Co, Ru, Pt, and total thicknesses of the heavy metal (HM) (t_{Co}, t_{Ru}, t_{Pt}, and t_{total}, respectively), where numbers in the parenthesis show the nominal thickness in nm. Ta/Pt(3)/[Co(0.5)/Pt(0.26)]$_4$/Co(0.5)/Ru(t_{Ru})/Co(0.5)/[Pt(0.26)/Co(0.5)]$_4$/Pt(3) (sample C) films with various t_{Ru} were also prepared in order to compare the oscillation period of interlayer exchange coupling as a function of t_{Ru} with Ta/Pt(3)/[Co(t_{Co})/Ru(t_{Ru})/Pt(t_{Pt})]$_3$/Co(t_{Co})/Ru(1)/Ta(2) (sample D) films. Because interlayer exchange coupling is largely related to the interface roughness between Co and Ru,[46] and Co, Pt, and Ru are solid-dissolved systems, the all films for studying the interlayer exchange coupling were not post-annealed.

Structural characterization was carried out using out-of-plane x-ray diffraction (XRD) with Cu-Kα radiation and cross-sectional high-resolution transmission electron microscopy (HR-TEM). Magnetic properties were measured using a vibrating sample magnetometer (VSM) at room temperature.

TABLE I. Sample structure (stack) prepared in this study.

Sample name	Structure of prepared films	t_{Co} (nm)	t_{Pt} (nm)	t_{Ru} (nm)	t_{total} (nm)
A	Ta(3)/Pt(3)/[Co(t_{Co})/Pt(t_{Pt})/Ru(t_{Ru})/Pt(t_{Pt})]$_n$/Co(t_{Co})/Ru(1)/Ta(2) ($n = 1$ *and* $n = 2$)	1.1, 1.3	0.6, 0.7, 0.8	0.7	1.9, 2.1, 2.3
B	Ta(3)/Pt(3)/[Co(t_{Co})/Ru(t_{Ru})/Pt(t_{Pt})]$_n$/Co(t_{Co})/Ru(1)/Ta(2) ($n = 1$ and $n = 2$)	0.9, 1.1, 1.3	0.3, 0.6, 1.0	0.7, 0.8	1.0, 1.3, 1.4, 1.7

Sample name	Structure of prepared films	t_{Ru} (nm)
C	Ta(3)/Pt(3)/[Co(0.5)/Pt(0.26)]$_4$/Co(0.5)/Ru(t_{Ru})/Co(0.5)/[Pt(0.26)/Co(0.5)]$_4$/Pt(3)	0.3, 0.35, 0.375, 0.4, 0.425, 0.45, 0.5, 0.6, 0.7, 0.8, 0.9, 1.0, 1.1, 1.2, 1.3, 1.4, 1.5, 1.6
D	Ta(3)/Pt(3)/[Co(0.9)/Ru(t_{Ru})/Pt(0.6)]$_2$/Co(0.9)/Ru(1)/Ta(2)	0.3, 0.35, 0.4, 0.45, 0.5, 0.6, 0.7, 0.8, 0.9, 1.0, 1.1, 1.2, 1.3, 1.4, 1.5, 1.6

Figure 1(c) shows the typical t_{Ru} dependence of XRD results for sample D ($t_{Ru} = 0.9$, 1.4, and 2.2 nm). The main peak positions are located between face-centered-cubic (fcc) Pt(111) and hexagonal Ru(0002), and the magnitude of intensity of main peaks increases with increasing t_{Ru}. Therefore, the crystal structure and the texture of Pt and Ru would be fcc (111) and hexagonal (0001) texture, respectively. The low angle peaks located at 2θ position between $2\theta = 36°$ and 41° have several satellite peaks as shown in Fig. 1(c). The observed satellite peaks in Fig. 1(c) reminiscent the designed multilayer structure. However, assuming the multilayer formation, the artificial thickness period ($\lambda_{multilayer}$) by using the 2θ distance between XRD peaks is estimated to be $\lambda_{multilayer} \sim 9.1$, 10.2, and 11.9 nm for the films with $t_{Ru} = 0.9$, 1.4, and 2.2 nm, respectively. These $\lambda_{multilayer}$ values are larger than the designed value of $\lambda_{multilayer} \sim 2.4$, 2.9, and 3.7 nm for [Co(0.9)/Ru(t_{Ru})/Pt(0.6)] and close to the total thicknesses of Pt(3)/[Co(0.9)/Ru(t_{Ru})/Pt(0.6)]$_2$/Co(0.9)/Ru(1.2) in sample D. Therefore, the possible reason for observing the satellite peaks in Fig. 1(c) might be flat and high-quality [Co(0.9)/Ru(t_{Ru})/Pt(0.6)]$_2$ multilayer HMs as observed in a high-quality semiconductor multilayer system.[47] However, these small diffraction peaks containing the satellite peaks were not very well defined. In the cases of Ta/Pt(3)/[Ru(0.6)/Pt(0.6)]$_7$ and Ta/Pt(3)/[Ru(1.1)/Pt(0.8)]$_5$ multilayer films, only the main peak located between fcc Pt(111) and hexagonal Ru(0002) is observed (not shown). Therefore, in any case, the crystal structures and textures of Pt and Ru in sample D with [Co(0.9)/Ru(t_{Ru})/Pt(0.6)]$_2$ multilayer HMs would be fcc (111) and hexagonal (0001) texture, respectively. This result is consistent with previous results.[48] To confirm the crystal structure and the texture of Pt and Ru, we observed a cross-sectional HR-TEM image.

Figure 1(d) shows the cross-sectional HR-TEM result for sample A ($n = 1$, $t_{Co} = 1.1$ nm, $t_{Pt} = 0.8$ nm, and $t_{Ru} = 0.7$ nm). Flat and epitaxially grown Pt/Co/[Pt/Ru/Pt]/Co/Ru with highly fcc (111)-textured Pt and hexagonal (0001)-textured Ru were observed. These results are consistent with the out-of-plane XRD results. As described before, the crystal structures of Ru and Pt are different (hexagonal and fcc, respectively); therefore, it is not clear if there is interlayer exchange coupling through Ru/Pt and Pt/Ru/Pt spacer layers. Therefore, we detailly studied interlayer exchange coupling through Ru/Pt and Pt/Ru/Pt spacer layers.

Figures 2(a)–2(c) and Figs. 2(d)–2(f) show the normalized out-of-plane and in-plane magnetization vs field (M–H) curves for sample C ($t_{Ru} = 0.4$, 0.8, and 1.2 nm) and sample D ($t_{Ru} = 0.4$, 0.8, and 1.2 nm), respectively. The red and blue arrows in the light pink color boxes in Figs. 2(a)–2(f) indicate the corresponding magnetization state; top and bottom arrows in Figs. 2(a)–2(c) represent the magnetization direction of the top and bottom Co layers; and top, middle, and bottom arrows in Figs. 2(d)–2(f) represent the magnetization direction of the top, middle, and bottom Co layers. As shown in Figs. 2(a) and 2(d), the remanence values of the magnetization at $H = 0$ T are nearly zero for both in-plane and out-of-plane magnetization directions for sample C ($t_{Ru} = 0.4$ nm); therefore, this indicates that the interlayer exchange coupling between Co layers through Ru($t_{Ru} = 0.4$) is antiferromagnetic, whereas the remanence value of the magnetization at $H = 0$ T is not zero for out-of-plane magnetization direction for sample D ($t_{Ru} = 0.4$ nm); therefore, this indicates that the interlayer exchange coupling between Co layers through Pt(0.6)/Ru($t_{Ru} = 0.4$) is ferromagnetic. For other t_{Ru}, the interlayer exchange coupling between Co layers through both Ru($t_{Ru} = 0.8$) and Pt(0.6)/Ru($t_{Ru} = 0.8$) is antiferromagnetic as shown in Figs. 2(b) and 2(e), and the interlayer exchange coupling between Co layers through both Ru($t_{Ru} = 1.2$) and Pt(0.6)/Ru($t_{Ru} = 1.2$) is ferromagnetic as shown in Figs. 2(c) and 2(f). In order to confirm the details of t_{Ru} dependence of the magnitude and sign of interlayer exchange coupling between Co layers through Ru and Pt/Ru spacer layers, we prepared the samples C and D with various t_{Ru} as shown in Table I. Figure 2(g) shows the magnitude of the interlayer exchange coupling ($|J_{ex}|$) as a function of t_{Ru} for samples C and D. The magnitude of $|J_{ex}|$ was evaluated using $|J_{ex}| = M_s\, t\, H_{ex}$,[48,49] where t and H_{ex} are the thickness of the Co/Pt layers and the exchange field described in Figs. 2(a), 2(b), and 2(e). The H_{ex} is defined as an intermediate value of the magnetic field in which the transition

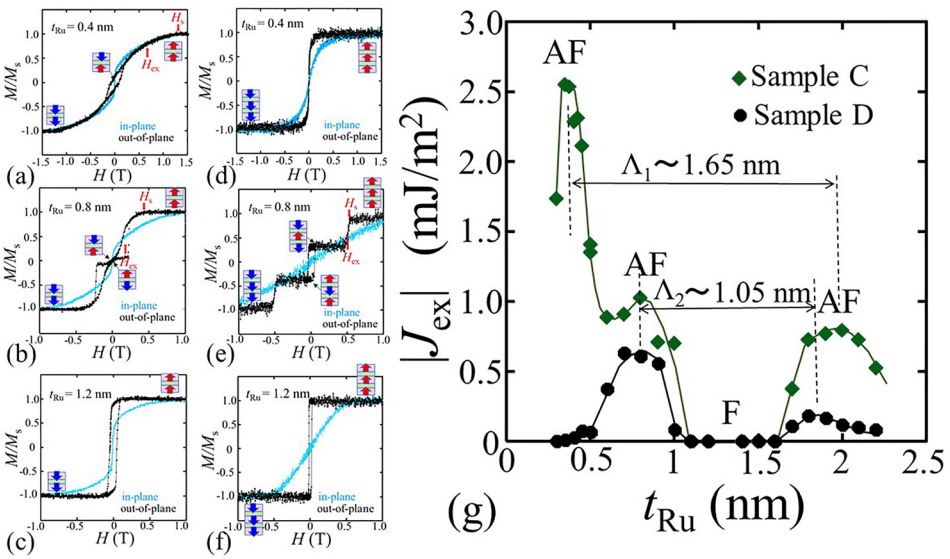

FIG. 2. (a)–(c) and (d)–(f) are normalized magnetization vs field (M–H) curves for sample C ($t_{Ru} = 0.4$, 0.8, and 1.2 nm) and sample D ($t_{Ru} = 0.4$, 0.8, and 1.2 nm), respectively. The red and blue arrows in the light pink color boxes in (a)–(f) indicate the corresponding magnetization state and the magnetization direction of each Co layers. (g) Magnitude of the interlayer exchange coupling ($|J_{ex}|$) as a function of Ru thickness (t_{Ru}) measured at room temperature in samples C and D. The one of oscillation periods ($\Lambda_1 = 1.65$ nm) of AF interlayer exchange coupling disappears in the case of interlayer exchange coupling through the Pt/Ru spacer layer (sample D).

from antiparallel magnetization sate to parallel magnetization state was observed. Transition field from antiparallel magnetization sate to parallel magnetization state in sample C ($t_{Ru} = 0.4$ nm) shown in Fig. 2(a) is not sharp compared to those in sample C ($t_{Ru} = 0.8$ nm) [Fig. 2(b)] and sample D ($t_{Ru} = 0.8$ nm) [Fig. 2(d)]. This would be because when t_{Ru} is thin, the non-uniformity in t_{Ru} due to the interface roughness between Co and Ru cannot be ignored. In the case of sample C ($t_{Ru} = 0.4$ nm), we deified the value of H_{ex} using same definition as described above. In the case of sample C, we can see that the t_{Ru} positions of the first AF, second AF, and third AF peaks are about 0.4, 0.8, and 2.0 nm, respectively. This result is consistent with the previous reports.[50–52] The reason for short period between the first and second AF peaks has not been fully understood and has been thought somewhat irregular behavior.[53] On the other hand, the t_{Ru} positions of the first AF and second AF peaks for sample D are 0.8 and 1.85 nm, respectively. Because the magnitude of $|J_{ex}|$ is nearly same between the second and third AF peaks in sample C, we think that the third AF peak observed at around $t_{Ru} = 2.0$ nm overlaps the third and fourth AF peaks in this system. Therefore, taking into account the extended Ruderman–Kittel–Kasuya–Yosida (RKKY) exchange model,[47,54,55] there are two spanning wave vectors (q_s) linking two points of Fermi surface with antiparallel velocities in the case of noble-metal spacer for sample C. On the other hand, there is only one q_s for sample D. According to the extended RKKY exchange model,[47,54,55] the oscillation period of AF interlayer exchange coupling Λ is given by $\Lambda = 2\pi/q_s$, where q_s is the spanning wave vector linking two point of Fermi surface with antiparallel velocities. The result of Fig. 2(g) shows that two oscillation periods of AF interlayer exchange coupling Λ would be about $\Lambda_1 \sim 1.65$ nm and $\Lambda_2 \sim 1.05$ nm for sample C, and $\Lambda_2 \sim 1.05$ nm for sample D. We think that the reason for the short period between the first and second AF peaks is due to the overlap of the AF oscillations with $\Lambda_1 \sim 1.65$ nm and $\Lambda_2 \sim 1.05$ nm in this system. The periods Λ_1 and Λ_2 are in good agreement with the periods of (1.48 and 1.71 nm) and (1.12 and 1.16 nm) that have been derived from the theoretical predicted extremal Fermi surface spanning vectors of Ru(0001).[53] Because the crystal structures of Pt and Ru are different from each other, the topological characteristic of the Fermi surfaces of Pt and Ru is different from each other, and J_{ex} with the period of Λ_1 cannot propagate through the Pt layer. On the other hand, we observed that J_{ex} with the period of Λ_2 can propagate through the Pt layer. In the case of interlayer exchange coupling through fcc spacer layer, such as Cu, Rh, Ir, and Pt/Ir,[40,56,57] the oscillation periods of these fcc metals are $\Lambda_{fcc} = 0.9 \sim 1.0$ nm. The observed $\Lambda_2 \sim 1.05$ nm in Ru/Pt and Pt/Ru/Pt systems is close to the value of Λ_{fcc}. Our result may indicate that the spanning wave vector with similar values in the different materials can propagate even between the materials with different crystal structures. More experimental and theoretical efforts would necessary for clarifying the reason for why the spanning wave vector of Λ_2 does not disappear and that of Λ_1 disappear in Ru/Pt and Pt/Ru/Pt systems.

From the application point of view, the MTJs with the first AF peak at $t_{Ru} \sim 0.4$ nm cannot use because the degradation of the AF interlayer exchange coupling was observed with the increasing annealing temperature, and the MTJs with the second AF peak at $t_{Ru} \sim 0.8$ nm have been usually used. Our result indicates that the reasons for this degradation in $t_{Ru} \sim 0.4$ nm sample and not degradation for $t_{Ru} \sim 0.8$ nm sample would be intrinsic. By increasing the annealing temperature in MTJs with the $[Co/Pt]_n/Co/Ru/[Co/Pt]_m$ synthetic pinned layer, not only an increase in interface roughness between Co and Ru but also an increase in interdiffusion between Pt and Ru would be occurred. These two would be the reasons of the degradation for the MTJs with the first AF peak. As shown in Fig. 2(g), the shift in the oscillation in the case of period Λ_2 was not observed. Moreover, the sign and intensity of the J_{ex} related to the period Λ_2 do not appear to oscillate with an increase in t_{Pt}. To confirm this interpretation, we measured the AF interlayer exchange coupling through Pt/Ru/Pt tri-layers in which this structure would be useful for the systematic investigation of the SOT on the AF structure shown in Figs. 1(a) and 1(b).

Figures 3(a) and 3(b) and Figs. 3(c) and 3(d) show the typical normalized out-of-plane and in-plane M–H curves for Ta/Pt(3)/$[Co(1.3)/Pt(t_{Pt})/Ru(0.7)/Pt(t_{Pt})]_2$/Co(1.3)/Ru(1)/Ta(2) (sample A, $n = 2$, $t_{Co} = 1.3$ nm, $t_{Ru} = 0.7$ nm, $t_{Pt} = 0.6$ and 0.7 nm) and Ta/Pt(3)/Co(1.3)/$Pt(t_{Pt})$/Ru(0.7)/$Pt(t_{Pt})$/Co(1.1)/Ru(1)/Ta(2) (sample A, $n = 1$, $t_{Co} = 1.3$ nm, $t_{Ru} = 0.7$ nm, and $t_{Pt} = 0.8$ and 0.6 nm) with Pt/Ru/Pt spacer tri-layers, respectively. As shown in Figs. 3(a) and 3(b), the magnitudes of the remanent magnetization in out-of-plane and in-plane M–H curves are almost 1/3 and zero, respectively, in the case of sample A ($n = 2$, $t_{Co} = 1.3$ nm, $t_{Ru} = 0.7$ nm, and $t_{Pt} = 0.6$ and 0.7 nm), which have three Co layers. The magnitudes of the remanent magnetization in out-of-plane and in-plane M–H curves are almost zero in sample A ($n = 1$, $t_{Co} = 1.3$ nm, $t_{Ru} = 0.7$ nm, and $t_{Pt} = 0.8$ and 0.6 nm) with two Co layers as shown in Figs. 3(c) and 3(d). Thus, we observed the AF interlayer exchange coupling through Pt/Ru/Pt tri-layers.

Figure 3(e) shows the log-log plot of $-J_{ex}$ as a function of $t_{total} = t_{Pt} + t_{Ru}$ for samples A and B ($n = 1$ and 2) with various t_{Co}, t_{Ru}, t_{Pt}, and t_{total} as shown in Table I. The $-J_{ex}$ values of the first, second, and third peak positions ($t_{Ru} = 0.4$, 0.8, and 2.0 nm) in sample C are also plotted in Fig. 3(e). As shown in Fig. 3(e), monotonous decrease in $-J_{ex}$ with an increase in t_{total} was observed except for the $-J_{ex}$ values of the third peak position ($t_{total} = t_{Ru} = 2.0$ nm) in sample C. As discussed before, the third AF peak observed in this system at around $t_{Ru} = 2.0$ nm would overlap the third and fourth AF peaks, which are related to the Λ_2 and Λ_1 oscillation periods, respectively. Therefore, the magnitude of the $-J_{ex}$ of the third peak position ($t_{Ru} = 2.0$ nm) in sample C would be larger than the other $-J_{ex}$ values observed in samples A and B ($n = 1$ and 2) with around $t_{total} \sim 2.0$ nm. As shown in Fig. 3(e), we observed AF interlayer exchange coupling through both Pt/Ru and Pt/Ru/Pt between wide thickness range of $1.0\ \text{nm} \leq t_{total} \leq 2.3$ nm. The observation of AF interlayer exchange coupling through wide thickness range of t_{total} and t_{Pt} ($0 \leq t_{Pt} \leq 0.8$ nm for Pt/Ru/Pt spacer layer and $0 \leq t_{Pt} \leq 1.0$ nm for Pt/Ru spacer layer) indicates that the sign of the interlayer exchange coupling does not oscillate in Pt. The black solid line in Fig. 3(e) is the result of least-square-fit using the equation $-J_{ex} \propto t_{total}^{-2}$. For the fitting, the data of the third peak position ($t_{Ru} = 2.0$ nm) in sample C were not used. The second power law of the t_{total} is the result of fitting assuming the RKKY interaction.[55,58] As shown in Fig. 3(e), the data fit well by using this equation except for the thicker t_{total} region. The inset of Fig. 3(e) shows the plot of $-J_{ex}$ as a function of total Pt thickness ($t_{Pt\,total}$) ($t_{Pt\,total} = 2\,t_{Pt}$ for sample A and $t_{Pt\,total} = t_{Pt}$ for sample B). The $-J_{ex}$ value of the second peak position ($t_{Ru} = 0.8$ nm) in sample C is also plotted in inset of Fig. 3(e). The blue solid line in inset of Fig. 3(e) is

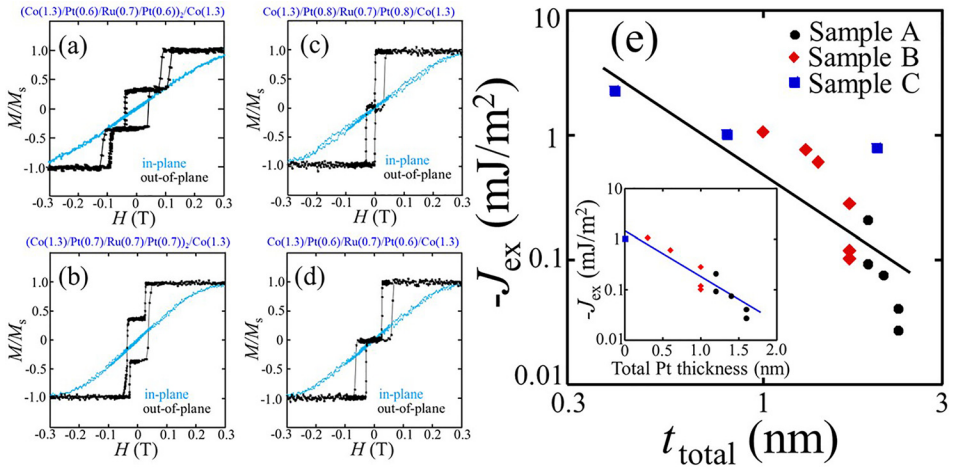

FIG. 3. (a) and (b) Normalized out-of-plane and in-plane *M–H* curves for Ta(3)/Pt(3)/[Co(1.3)/Pt(t_{Pt})/Ru(0.7)/Pt(t_{Pt})]$_2$/Co(1.3)/Ru(1)/Ta(2) (sample A, $n = 2$, $t_{Co} = 1.3$ nm, $t_{Ru} = 0.7$ nm, and $t_{Pt} = 0.6$ and 0.7 nm, respectively). (c) and (d) Normalized out-of-plane and in-plane *M–H* curves for Ta(3)/Pt(3)/Co(1.3)/Pt(t_{Pt})/Ru(0.7)/Pt(t_{Pt})/Co(1.1)/Ru(1)/Ta(2) (sample A, $n = 1$, $t_{Co} = 1.3$ nm, $t_{Ru} = 0.7$ nm, and $t_{Pt} = 0.8$ and 0.6 nm, respectively). AF interlayer exchange coupling through Pt/Ru/Pt tri-layers was observed. (e) Log–log plot of AF interlayer exchange coupling ($-J_{ex}$) as a function of $t_{total} = t_{Pt} + t_{Ru}$ for samples A and B ($n = 1$ and 2) with various t_{Co}, t_{Ru}, t_{Pt}, and t_{total}. The $-J_{ex}$ values of the first, second, and third peak positions ($t_{Ru} = 0.4$, 0.8, 2.0 nm) in sample C are also plotted in (e). The black solid line is the result of least-square-fit using the equation $-J_{ex} \propto t_{total}^{-2}$. Inset of (e) is the plot of $-J_{ex}$ as a function of total Pt thickness. The blue solid line in inset of (e) is the fitted result using the equation: $-J_{ex} \propto \exp(a - b\, t_{Pt\ total})$, where a and b are fitting parameters ($a = 0.37$, $b = 2.05$).

the fitted result using the equation $-J_{ex} \propto \exp(a - b\, t_{Pt\ total})$, where a and b are fitting parameters ($a = 0.37$, $b = 2.05$). The $-J_{ex}$ vs $t_{Pt\ total}$ plot in inset of Fig. 3(e) shows exponential decay rather than $t_{Pt\ total}^{-2}$ decay. In the Pt layer, the decrease in the magnitude of $|J_{ex}|$ does not seem to follow the second power law. This might be the reason for the discrepancy in the thicker t_{total} region shown in Fig. 3(e). On the other hand, Ref. 48 shows the same tendency (the decrease in the magnitude of $|J_{ex}|$ does not follow the second power law in the thicker t_{Ru} region). They conclude that this discrepancy in the thicker t_{Ru} region would be related to the temperature dependence of the magnitude of $-J_{ex}$. Further experimental and theoretical efforts are necessary to fully understand the magnitude of interlayer exchange coupling through Pt/Ru/Pt and Pt/Ru layers. In any way, we observed the relatively large magnitude of $|J_{ex}|$ in the wide thickness range of the nonmagnetic spacer of Pt/Ru/Pt and Pt/Ru. These results would be useful for the SOT switching on the AF structure.

In the synthetic AF coupling layer with completely compensated magnetization, evaluation of the efficiency of SHE is difficult and determination of SOT efficiencies in synthetic AF remains elusive.[59,60] More recently reported papers show enhancement of SHE in the synthetic AF coupling system.[61,62] One of them[62] uses Pt located outside the synthetic AF coupling layer to evaluate SOT efficiency. Another paper[61] evaluates the SOT efficiency using the synthetic AF coupling layer with uncompensated magnetization with three ferromagnetic layers. Model calculations based on the Landau–Lifshitz Gilbert equation[61] show that the presence of antiferromagnetic coupling can increase the SOT due to the existence of the exchange coupling field (H_{ex}) defined in Fig. 2. However, the model could not explain the experimentally observed magnitude of the SHE enhancement in the synthetic AF coupling layer.[61] They conclude that there are other sources of SOT besides H_{ex} that may account for the highly efficient SOT acting on the synthetic AF coupling layer. Particularly, for the ferromagnet/Pt/Ru/Pt/ferromagnet system we proposed in this study, the magnitude of H_{ex} changes depending on the film thicknesses of Pt and Ru as shown in Fig. 3(e) and the efficiency of SHE would also change because the observed AF thickness range of $0 \leq t_{Pt} \leq 0.8$ nm is shorter than spin diffusion length (λ_{PT}) in Pt ($\lambda_{PT} \geq 1$ nm).[33,42–45,63,64] Therefore, it is expected that the result of t_{Pt} dependence of the SOT efficiency in the ferromagnet/Pt/Ru/Pt/ferromagnet system will show more complex result. Further experimental and theoretical efforts in the synthetic AF coupling layer with completely compensated and uncompensated magnetization and/or with various magnitudes of exchange coupling strength and/or with in-plane and out-of-plane magnetization are required to clarify the origin of the SOT in the synthetic AF coupling layer.

In summary, we have investigated the interlayer exchange coupling in Co/nonmagnetic spacer layer/Co systems with Pt/Ru and Pt/Ru/Pt nonmagnetic spacer layers, and compared to that with the Ru nonmagnetic spacer layer. The AF interlayer exchange coupling for the Pt/Ru/Pt nonmagnetic spacer layer samples was observed in the wide ranges of Pt thickness ($0 \leq t_{Pt} \leq 0.8$ nm) and total thickness of nonmagnetic spacer layer thickness ($1.0 \leq t_{total} \leq 2.3$ nm), which is available for the studying AF spintronics using current-induced SOT switching. Moreover, the existence of two oscillation periods of AF interlayer exchange coupling ($\Lambda_1 \sim 1.65$ nm and $\Lambda_2 \sim 1.05$ nm) in the case of the Ru spacer layer and the existence of the AF interlayer exchange coupling with the oscillation period of $\Lambda_2 \sim 1.05$ nm and disappearance of that with the oscillation period of $\Lambda_1 \sim 1.65$ nm in the case of fcc Pt(111)/hexagonal Ru(0001) and fcc Pt(111)/hexagonal Ru(0001)/fcc Pt(111) spacer layers were observed. We expect that the Pt/Ru/Pt spacer layer with the oscillation period of $\Lambda_2 \sim 1.05$ nm will pave a way to the AF spintronics based on the multilayer systems.

The authors express their gratitude to T. Miyazaki for the measurement of HR-TEM images. This work was supported by the CIES Consortium, JST OPERA (Grant No. JPMJOP1611), and JSPS KAKENHI (Grant Nos. JP19H00844 and JP21K18189).

DATA AVAILABILITY

The data that support the findings of this study are available from the corresponding author upon reasonable request.

REFERENCES

[1]T. Jungwirth, X. Marti, P. Wadley, and J. Wunderlich, Nat. Nanotechnol. **11**, 231 (2016).
[2]V. Baltz, A. Manchon, M. Tsoi, T. Moriyama, T. Ono, and Y. Tserkovnyak, Rev. Mod. Phys. **90**, 015005 (2018).
[3]Z. Wei, A. Sharma, A. S. Nunez, P. M. Haney, R. A. Duine, J. Bass, A. H. MacDonald, and M. Tsoi, Phys. Rev. Lett. **98**, 116603 (2007).
[4]See L. Néel, http://www.nobelprize.org/nobel_prizes/physics/laureates/1970/neel-lecture.pdf for information about the Nobel Prize in Physics 1970.
[5]D. Houssameddine, J. F. Sierra, D. Gusakova, B. Delaet, U. Ebels, L. D. Buda-Prejbeanu, M. C. Cyrille, B. Dieny, B. Ocker, J. Langer, and W. Maas, Appl. Phys. Lett. **96**, 072511 (2010).
[6]K. Tanaka, T. Moriyama, M. Nagata, T. Seki, K. Takanashi, S. Takahashi, and T. Ono, Appl. Phys. Exp. **7**, 063010 (2014).
[7]P. Wadley, B. Howells, J. Železný, C. Andrews, V. Hills, R. P. Campion, V. Novák, K. Olejník, F. Maccherozzi, S. S. Dhesi, S. Y. Martin, T. Wagner, J. Wunderlich, F. Freimuth, Y. Mokrousov, J. Kuneš, J. S. Chauhan, M. J. Grzybowski, A. W. Rushforth, K. Edmond *et al.*, Science **351**, 587 (2016).
[8]T. Moriyama, K. Oda, T. Ohkochi, M. Kimata, and T. Ono, Sci. Rep. **8**, 14167 (2018).
[9]S. Y. Bodnar, L. Šmejkal, I. Turek, T. Jungwirth, O. Gomonay, J. Sinova, A. A. Sapozhnik, H. J. Elmers, M. Klaüi, and M. Jourdan, Nat. Commun. **9**, 348 (2018).
[10]T. Moriyama, W. Zhou, T. Seki, K. Takanashi, and T. Ono, Phys. Rev. Lett. **121**, 167202 (2018).
[11]X. Z. Chen, R. Zarzuela, J. Zhang, C. Song, X. F. Zhou, G. Y. Shi, F. Li, H. A. Zhou, W. J. Jiang, F. Pan, and Y. Tserkovnyak, Phys. Rev. Lett. **120**, 207204 (2018).
[12]W. Zhou, T. Seki, T. Kubota, G. E. W. Bauer, and K. Takanashi, Phys. Rev. Mater. **2**, 094404 (2018).
[13]M. Meinert, D. Graulich, and T. Matalla-Wagner, Phys. Rev. Appl. **9**, 064040 (2018).
[14]M. J. Grzybowski, P. Wadley, K. W. Edmonds, R. Beardsley, V. Hills, R. P. Campion, B. L. Gallagher, J. S. Chauhan, V. Novak, T. Jungwirth, F. Maccherozzi, and S. S. Dhesi, Phys. Rev. Lett. **118**, 057701 (2017).
[15]A. A. Sapozhnik, M. Filianina, S. Y. Bodnar, A. Lamirand, M. A. Mawass, Y. Skourski, H. J. Elmers, H. Zabel, M. Kläui, and M. Jourdan, Phys. Rev. B **97**, 134429 (2018).
[16]H. Masuda, T. Seki, Y.-C. Lau, T. Kubota, and K. Takanashi, Phys. Rev. B **101**, 224413 (2020).
[17]L. Liu, C.-F. Pai, Y. Li, H. W. Tseng, D. C. Ralph, and R. A. Buhrman, Science **336**, 555 (2012).
[18]G. Yu, P. Upadhyaya, Y. Fan, J. G. Alzate, W. Jiang, K. L. Wong, S. Takei, S. A. Bender, L.-T. Chang, Y. Jiang, M. Lang, J. Tang, Y. Wang, Y. Tserkovnyak, P. K. Amiri, and K. L. Wang, Nat. Nanotechnol. **9**, 548 (2014).
[19]W. Jiang, P. Upadhyaya, W. Zhang, G. Yu, M. B. Jungfleisch, F. Y. Fradin, J. E. Pearson, Y. Tserkovnyak, K. L. Wang, O. Heinonen, S. G. E. Velthuis, and A. Hoffmann, Science **349**, 283 (2015).
[20]P. P. J. Haazen, E. Mure, J. H. Franken, R. Lavrijsen, H. J. M. Swagten, and B. Koopmans, Nat. Mater. **12**, 299 (2013).
[21]A. Chernyshov, M. Overby, X. Liu, J. K. Furdyna, Y. Lyanda-Geller, and L. P. Rokhinson, Nat. Phys. **5**, 656 (2009).
[22]I. M. Miron, K. Garello, G. Gaudin, P. –J. Zermatten, M. V. Costache, S. Auffret, S. Bandiera, B. Rodmacq, A. Schuhl, and P. Gambardella, Nature **476**, 189 (2011).
[23]J. Kim, J. Sinha, M. Hayashi, M. Yamanouchi, S. Fukami, T. Suzuki, S. Mitani, and H. Ohno, Nat. Mater. **12**, 240 (2013).
[24]S. Fukami, T. Anekawa, C. Zhang, and H. Ohno, Nat. Nanotechnol. **11**, 621 (2016).
[25]K.-S. Lee, S.-W. Lee, B.-C. Min, and K.-J. Lee, Appl. Phys. Lett. **104**, 072413 (2014).
[26]K. Garello, C. O. Avci, I. M. Miron, M. Baumgartner, A. Ghosh, S. Auffret, O. Boulle, G. Gaudin, and P. Gambardella, Appl. Phys. Lett. **105**, 212402 (2014).
[27]C. Zhang, S. Fukami, H. Sato, F. Matsukura, and H. Ohno, Appl. Phys. Lett. **107**, 012401 (2015).
[28]M.-H. Nguyen, C.-F. Pai, K. X. Nguyen, D. A. Muller, D. C. Ralph, and R. A. Buhrman, Appl. Phys. Lett. **106**, 222402 (2015).
[29]S. V. Aradhya, G. E. Rowlands, J. Oh, D. C. Ralph, and R. A. Buhrman, Nano Lett. **16**, 5987 (2016).
[30]M. Baumgartner, K. Garello, J. Mendil, C. O. Avci, E. Grimaldi, C. Murer, J. Feng, M. Gabureac, C. Stamm, Y. Acremann, S. Finizio, S. Wintz, J. Raabe, and P. Gambardella, Nanotechnology **12**, 980 (2017).
[31]Y. Kato, Y. Saito, H. Yoda, T. Inokuchi, S. Shirotori, N. Shimomura, S. Oikawa, A. Tiwari, M. Ishikawa, M. Shimizu, B. Altansargai, H. Sugiyama, K. Koi, Y. Ohsawa, and A. Kurobe, Phys. Rev. Appl. **10**, 044011 (2018).
[32]Y. Saito, N. Tezuka, S. Ikeda, H. Sato, and T. Endoh, Appl. Phys. Exp. **12**, 053008 (2019).
[33]Y. Saito, N. Tezuka, S. Ikeda, H. Sato, and T. Endoh, AIP. Adv. **9**, 125312 (2019).
[34]Y. Saito, N. Tezuka, S. Ikeda, H. Sato, and T. Endoh, Appl. Phys. Lett. **116**, 132401 (2020).
[35]H. Honjo, T. V. A. Nguen, T. Watanabe, T. Nasuno, C. Zhang, T. Tanigawa, S. Miura, H. Inoue, M. Niwa, T. Yoshiduka, Y. Noguchi, M. Yasuhira, A. Tamakoshi, M. Natsui, Y. Ma, H. Koike, Y. Takahashi, K. Furuya, H. Shen, S. Fukami, H. Sato, S. Ikeda, T. Hanyu, H. Ohno, and T. Endoh, IEDM Tech. Dig. **28**, 5 (2019).
[36]M. Natsui, A. Tamakoshi, H. Honjo, T. Watanabe, T. Nasuno, C. Zhang, T. Tanigawa, H. Inoue, M. Niwa, T. Yoshiduka, Y. Noguchi, M. Yasuhira, Y. Ma, H. Shen, S. Fukami, H. Sato, S. Ikeda, H. Ohno, T. Endoh, and T. Hanyu, IEEE J. Solid-State Circuits **56**, 116 (2021), available at https://ieeexplore.ieee.org/document/9288784.
[37]P. Grünberg, R. Schreiber, Y. Pang, M. B. Brodsky, and H. Sowers, Phys. Rev. Lett. **57**, 2442 (1986).
[38]C. Carbone and S. F. Alvarado, Phys. Rev. B **36**, 2433 (1987).
[39]Z. Dai, W. Liu, X. Zhao, L. Liu, and Z. Zhang, ACS Appl. Electron. Mater. **3**, 611 (2021).
[40]Y. Saito, N. Tezuka, S. Ikeda, H. Sato, and T. Endoh, Phys. Rev. B **104**, 064439 (2021).
[41]Z. Wen, J. Kim, H. Sukegawa, M. Hayashi, and S. Mitani, AIP Adv. **6**, 056307 (2016).
[42]T. Fache, J. C. Rojas-Sanchez, L. Badie, S. Mangin, and S. Petit Watelot, Phys. Rev. B **102**, 064425 (2020).
[43]R. Ramaswamy, Y. Wang, M. Elyasi, M. Motapothula, T. Venkatesan, X. Qiu, and H. Yang, Phys. Rev. Appl. **8**, 024034 (2017).
[44]M. Isasa, E. Villamor, L. E. Hueso, M. Gradhand, and F. Casanova, Phys. Rev. B **91**, 024402 (2015).
[45]L. Wang, R. J. H. Wesselink, Y. Liu, Z. Yuan, K. Xia, and P. J. Kelly, Phys. Rev. Lett. **116**, 196602 (2016).
[46]P. Bruno and C. Chappert, Phys. Rev. Lett. **67**, 1602 (1991).
[47]K. W. Shin, S. Song, H.-W. Kim, G.-D. Lee, and E. Yoon, Jpn. J. Appl. Phys., Part 1 **57**, 065504 (2018).
[48]P. J. H. Bloemen, H. W. Vankesteren, H. J. M. Swagten, and W. J. M. Dejonge, Phys. Rev. B **50**, 13505 (1994).
[49]W. Folkerts, J. Magn. Magn. Mater. **94**, 302 (1991).
[50]S. S. P. Parkin, N. More, and K. P. Roche, Phys. Rev. Lett. **64**, 2304 (1990).
[51]S. Bandiera, R. C. Sousa, S. Auffret, B. Rodmacq, and B. Dieny, Appl. Phys. Lett. **101**, 072410 (2012).
[52]K. Yakushiji, H. Kubota, A. Fukushima, and S. Yuasa, Appl. Phys. Exp. **8**, 083003 (2015).
[53]M. D. Stiles, Phys. Rev. B **48**, 7238 (1993).
[54]P. Bruno, J. Phys.: Condens. Matter **11**, 9403 (1999).
[55]Y. Yafet, Phys. Rev. B **36**, 3948 (1987).
[56]S. S. P. Parkin, Phys. Rev. Lett. **67**, 3598 (1991).
[57]K. Yakushiji, A. Sugihara, A. Fukushima, H. Kubota, and S. Yuasa, Appl. Phys. Lett. **110**, 092406 (2017).

[58]W. Baltensperger and J. S. Helman, Appl. Phys. Lett. **57**, 2954 (1990).
[59]C. Bi, H. Almasi, K. Price, T. Newhouse-Illige, M. Xu, S. R. Allen, X. Fan, and W. Wang, Phys. Rev. B **95**, 104434 (2017).
[60]G. Y. Shi, C. H. Wan, Y. S. Chang, F. Li, X. J. Zhou, P. X. Zhang, J. W. Cai, X. F. Han, F. Pan, and C. Song, Phys. Rev. B **95**, 104435 (2017).
[61]Y. Ishikuro, M. Kawaguchi, T. Taniguchi, and M. Hayashi, Phys. Rev. B **101**, 014404 (2020).
[62]P. X. Zhang, L. Y. Liao, G. Y. Shi, R. Q. Zhang, H. Q. Wu, Y. Y. Wang, F. Pan, and C. Song, Phys. Rev. B **97**, 214403 (2018).
[63]J.-C. Rojas-Sánchez, N. Reyren, P. Laczkowski, W. Savero, J.-P. Attané, C. Deranlot, M. Jamet, J.-M. George, L. Vila, and H. Jaffrès, Phys. Rev. Lett. **112**, 106602 (2014).
[64]C. Stamm, C. Murer, M. Berritta, J. Feng, M. Gabureac, P. M. Oppeneer, and P. Gambardella, Phys. Rev. Lett **119**, 087203 (2017).